JOURNAL OF MAGNETIC RESONANCE, Series A 115, 127–130 (1995)

Spin-Polarized ^{129}Xe Gas Imaging of Materials*

Y.-Q. SONG, H. C. GAEDE, T. PIETRAß, G. A. BARRALL, G. C. CHINGAS, M. R. AYERS,† AND A. PINES

Materials Sciences Division and †Energy and Environment Division, Lawrence Berkeley Laboratory, Berkeley, California 94720; and Department of Chemistry, University of California, Berkeley, California 94720

Received April 5, 1995

Nuclear magnetic resonance is an established technique for imaging and microscopy in a wide variety of systems (*1*). In parallel with the substantial progress in line narrowing for the purpose of solids imaging (*2*), one attractive method is to saturate the sample with a high-sensitivity contrast agent and thereby obtain a "negative" image, which depicts the void structure. Proton-containing solvents, such as water, are ideal contrast agents due to their high intrinsic sensitivity, but in some cases they can react with the material and modify its structure. In these cases inert gases such as xenon, which is used extensively in NMR as a probe of its surroundings (*3, 4*), are an attractive alternative, and despite their low intrinsic sensitivity due to low spin density, there have been several successful gas imaging studies. Lizak, Conradi, and Fry imaged C_2F_6 gas imbibed into a porous ceramic matrix–ceramic fiber composite (*5*). As part of a study to ascertain the feasibility of studying nuclei in low concentrations with a whole-body imaging spectrometer, Pfeffer and Lutz imaged a xenon–oxygen mixture (*6*). One approach to overcoming the limitations of low sensitivity, for example, in surface-selective NMR, is the use of optically polarized gases, for example, xenon or helium, which can reach spin polarizations 4–5 orders of magnitude greater than those of the thermally polarized gases (*7, 8*). This method, based on the pioneering laser polarization work of Happer and co-workers at Princeton (*9, 10*), has been used to obtain biological images of the gas space in rat and guinea pig lungs (*11, 12*). Here, we present our preliminary results of polarized xenon gas imaging of materials, in particular, a structured phantom sample with a spatial resolution of approximately 0.1 mm and a water-sensitive sample of aerogel.

Optically polarized xenon is obtained by laser optical pumping of Rb followed by spin exchange between the Rb and ^{129}Xe. ^{129}Xe polarizations as high as 30% have been reported (*13*), corresponding to an enhancement of 10^5 over the equilibrium polarization achieved in a magnetic field of 4.2 T. The density of gaseous xenon at 1 atm pressure is 4×10^{-5} mol/cm^3. With the polarizations attainable through optical pumping, the magnetization density of polarized xenon becomes comparable to the proton magnetization in water, 0.1 mol/cm^3, making it possible to attain images of a gas without the need for extensive signal averaging.

The details of our optical-pumping apparatus have been published previously (*14*) and only a brief description is outlined below. The central part of the optical-pumping apparatus is the pumping cell, a 35 cm^3 glass cylinder connected to the NMR sample cell and the vacuum pumps via glass tubing and detachable joints. Several stopcocks facilitate convenient gas handling. All parts of the glassware are carefully treated with a siliconizing agent (SurfaSil, Pierce Scientific) to reduce the surface relaxation of ^{129}Xe (*15*). This treatment is of particular importance for the pumping cell since the surface relaxation by wall collisions is also a source of depolarization for Rb, the immediate source of spin polarization for xenon. In these experiments a magnetic field of ~30 G is provided by a pair of Helmholtz coils.

The entire optical-pumping apparatus is mounted on a laser table. The pumping cell is irradiated along the direction of the magnetic field for typically 30 minutes using a Ti-Sapphire laser (Schwartz Electro Optics), which is pumped by a 10 W Ar^+ laser (Coherent, Innova 310). The typical output power of the Ti-Sapphire laser is 1–1.5 W at the D_1 transition of Rb (795 nm). The helicity of the light is adjusted by a quarter-wave plate to be either σ^+ or σ^-. The pumping cell is maintained at 70–80°C using flowing nitrogen gas. An elevated temperature increases the density of Rb atoms in the vapor phase, allowing for optimal absorption of the laser light. Before any NMR experiments are begun, the xenon is separated from the Rb by allowing the pumping cell to cool to ambient temperature, thus condensing the Rb. Xenon gas is then allowed to expand into the sample region. The sample cell is closed, disconnected from the pumping apparatus, and moved to the imaging spectrometer. Enriched ^{129}Xe gas (80% ^{129}Xe, EG + G Mound) was used in all experiments described below. The xenon gas pressure used in the sample cell ranged from 1 to 3 atm.

The imaging experiments were performed on a commercial microimaging spectrometer (Quest 4400, Nalorac Cryogenics, Inc.) using cylindrical microimaging gradients (Nalorac Cryogenics, Inc.) and a home-built probe. At the

* Presented in part at the 36th ENC, March 26–30, 1995, Boston, Massachusetts.

1064-1858/95 $12.00

magnetic field of 4.3 T, the ^{129}Xe resonance frequency is 51 MHz. A standard FLASH (*f*ast *l*ow-*a*ngle *sh*ot) sequence (*16*), shown in Fig. 1, was used for the two-dimensional imaging experiments. The tipping angle used was 10° and the magnetic field gradient strength was 3.8 kHz/mm. Sixty-four phase-encoding steps were used to produce a 128 × 64 time-domain data set. A xenon image was taken of a phantom composed of three nested glass tubes with outside diameters of 9, 6, and 4 mm. Because of the way these tubes rest within each other, they form gaps varying continuously in diameter, providing a convenient gauge for image resolution. Figure 2 shows a sketch of the phantom together with a cross-sectional xenon image, indicating a spatial resolution of about 0.1 mm. The three tubes were also carefully treated with SurfaSil prior to the experiment to reduce relaxation effects. Indeed, we found that the tubes did not noticeably increase the relaxation rate of xenon magnetization during imaging experiments.

An alternative to using images for the characterization of small-scale heterogeneities is the use of NMR Patterson functions (*17*). These NMR Patterson functions are analogous to the density autocorrelation functions of X-ray diffraction, except that nuclear rather than electronic density provides contrast and the spatial resolution is determined by magnetic field gradient strength rather than the momentum transfer in X-ray scattering. Figure 3 shows the NMR image and the Patterson function, showing the radial density distribution, of a bundle of hollow Teflon tubes. Both the image and the Patterson function are consistent with an inner diameter of ~0.3 mm, limited by the digital resolution and the overlapping signals caused by the misalignment of the Teflon tubes over the slice-selection length of 15 mm.

An estimate of the effects of xenon gas diffusion on imaging resolution can be made. During the application of the gradient pulses, lasting 1.16 ms, the root-mean-squared dis-

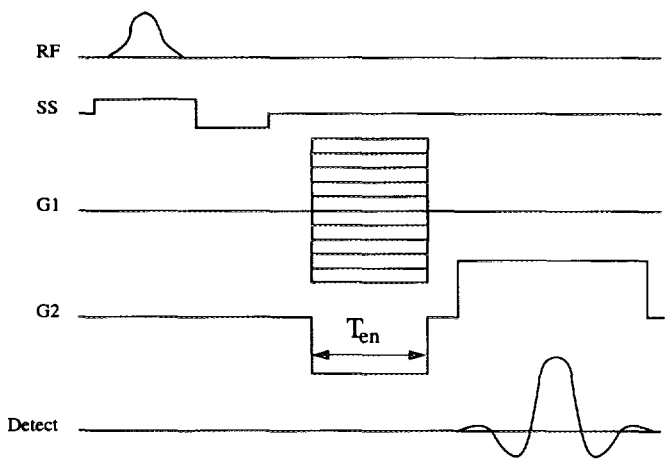

FIG. 1. A schematic of the FLASH imaging sequence. Typical encoding time T_{en} was 580 μs using a read gradient G_2 of 3.8 kHz/mm. Acquisitions were made for 64 phase-encoding gradient pulses G_1.

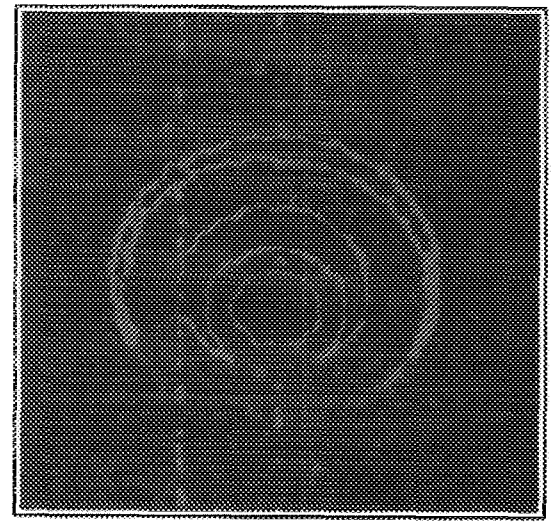

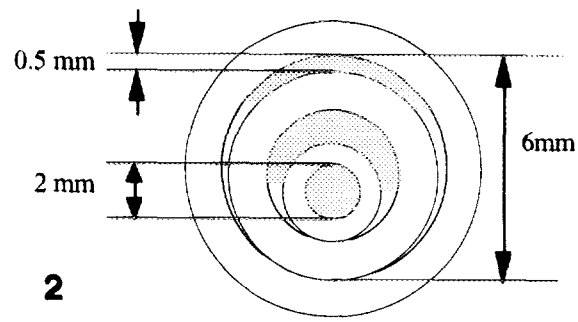

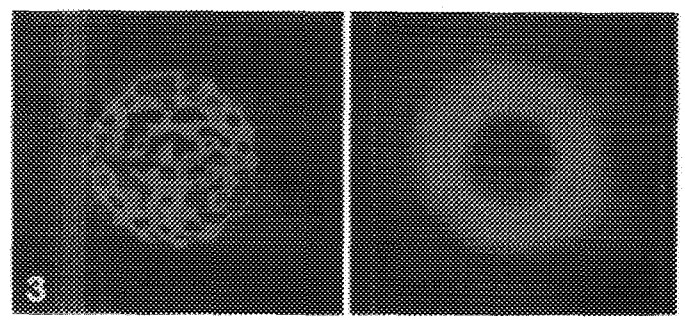

FIG. 2. Two-dimensional image of a phantom made of three nested glass tubes. The sizes of the tubes are shown in the cross-sectional sketch. Since the three tubes rest within each other, the gaps between tubes (shaded area in the sketch) continuously change from 0 to 2 mm. Areas in red, green, and blue have high, intermediate, and low signal intensity, respectively.

FIG. 3. (a) Two-dimensional image (box dimensions, 13 × 12 mm) of ^{129}Xe gas in bundled Teflon tubes, with 1 mm o.d. and 0.3 mm i.d. Areas in red, green, and blue have high, intermediate, and low signal intensity, respectively. The overlapping signals are due to the misalignment of the Teflon tubes over the slice-selection length of 15 mm. (b) Patterson function (box dimensions, 13 × 12 mm) of same sample showing polarized xenon density distribution function.

placement at the pressures at which the phantom image was acquired is ~60 μm, smaller than the resolution achieved. However, the root-mean-squared displacement for 1 atm of xenon is 100 μm, so the diffusion limit to resolution is controlled by experimental parameters. In fact, fast diffusion of xenon gas can be advantageous in some cases, as diffusion of xenon from outside the selected slice replenishes magnetization destroyed by previous RF pulses. A delay of 5–10 seconds between acquisitions was sufficient to allow polarized ^{129}Xe to diffuse into the sample region, thus further enhancing the signal-to-noise ratio. Moreover, the ability to perform multiple acquisitions can be exploited for phase cycling and signal averaging.

One important application of gas imaging is the study of solid materials that are chemically sensitive to water and other liquids, or which may in some other way be altered upon exposure to moisture. Examples of such materials include food products, polymers, catalysts, and aerogels. Aerogels are a class of porous materials typically based on silica (*18*), other metal oxides (*19*), or organic polymers (*20*). Their preparation involves standard sol–gel hydrolysis and condensation steps followed by solvent exchange and supercritical drying (*21*). The supercritical drying step eliminates the destructive forces caused by liquid–vapor interfaces and preserves the original gel structure. For silica aerogels, this structure consists of silica particles 2–5 nm in diameter, linked in a meandering three-dimensional network. Typical apparent bulk densities range from 0.003 to 0.25 g/cm^3. Specific surface areas as high as 800–1000 m^2/g (~100 m^2/cm^3) are common. The remainder of the bulk volume of an aerogel is an open pore network. Pore diameters (derived from adsorption/desorption isotherms) range from 2 to 100 nm, with a mean of ~20 nm. Many of the proposed applications of aerogels require a detailed understanding of gas dynamics within the aerogel matrix. NMR imaging may provide valuable information concerning gas diffusivity and dynamics in aerogel as well as images of the uniformity and defects of the material itself.

We have performed imaging experiments in order to study xenon gas penetration into a sample of aerogel prepared by basic catalysis of tetraethyl orthosilicate and dried using supercritical carbon dioxide. The final density of the sample was 0.1 g/cm^3. For this experiment, the optically enhanced ^{129}Xe was stored separately and was not introduced into the sample region until immediately before acquisition of images. The aerogel sample was a cylinder 4 mm in diameter and 7 mm in length and was prepared by forcing a glass tube into a larger block of the aerogel material. One-dimensional images are shown in Fig. 4, taken at various times after xenon was released into the sample region. A 90° pulse was used for each experiment. The two high ridges in the spectra indicate the edges of the sample. The overall shapes of all the spectra are similar, indicating that gas penetration occurred before our first acquisition, about three seconds after xenon

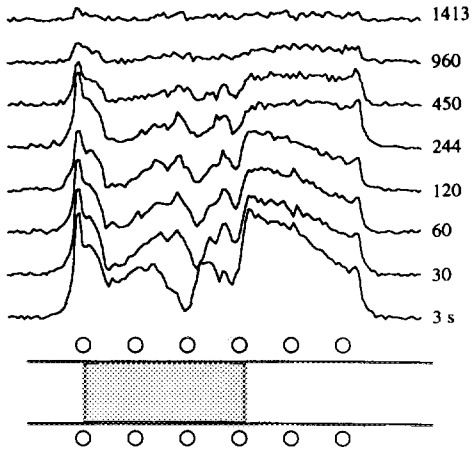

FIG. 4. One-dimensional images of ^{129}Xe penetration into an aerogel sample. The schematic shows the arrangement of the sample (dimensions, 4 mm diameter, 7 mm length), the radiofrequency coil, and the glass-tube container. Images were taken at increasing delay times after xenon entered the sample region. Note the consistently low-intensity areas within the sample, indicative of sample or penetration inhomogeneity.

gas entered the sample region. However, all the images show low intensity in a few regions, suggesting that xenon gas does not penetrate into these parts of the sample easily and that the sample is not uniform on a millimeter length scale, demonstrating the applicability of this technique to the study of porous and heterogeneous materials.

In conclusion, we have shown that using optically polarized ^{129}Xe as a contrast agent, one may obtain NMR images with a resolution of 0.1 mm in FLASH experiments. Fast diffusion of xenon may actually improve the images acquired by allowing fresh ^{129}Xe magnetization to replenish the polarization lost due to RF pulses. We have also demonstrated the possible use of this technique for the investigation of material inhomogeneity and perhaps sample morphology, which, for certain samples, may not be possible by NMR imaging of water. Efforts toward alternative imaging methods, including echo-planar imaging (*22, 23*), are currently underway in our program of applying this technique to studying structure and gas dynamics in a range of materials.

ACKNOWLEDGMENTS

The authors thank J. A. Jones for carefully reading and commenting on the manuscript. Y.Q.S. acknowledges support from the Miller Research Fellowship from the Miller Institute for Basic Research in Science. This work is supported by the Director, Office of Basic Energy Sciences, Materials Science Division of the U.S. Department of Energy, and M.R.A. is supported by the Assistant Secretary for Conservation and Renewable Energy, Advanced Industrials Program of the Advanced Industrial Concepts Division, Office of Industrial Technologies of the U.S. Department of Energy, under Contract DE AC03-76SF00098.

REFERENCES

1. P. T. Callaghan, "Principles of Nuclear Magnetic Resonance Microscopy," Clarendon Press, Oxford, 1991.

2. P. Blümler and B. Blümich, *in* "Solid-State NMR. I. Methods" (P. Diehl, E. Fluck, H. Guenther, R. Kosfeld, and J. Seelig, Eds.), Springer-Verlag, New York/Berlin, 1994.
3. T. Ito and J. Fraissard, *in* "Proceedings, 5th International Conference on Zeolites," p. 150, Heyden, Naples, 1980.
4. J. A. Ripmeester and D. W. Davidson, *Bull. Magn. Reson.* **2,** 139 (1981).
5. M. J. Lizak, M. S. Conradi, and C. G. Fry, *J. Magn. Reson.* **95,** 548 (1991).
6. M. Pfeffer and O. Lutz, *J. Magn. Reson. A* **108,** 106 (1994).
7. D. Raftery, H. Long, T. Meersmann, P. J. Grandinetti, L. Reven, and A. Pines, *Phys. Rev. Lett.* **66,** 584 (1991).
8. H. W. Long, H. C. Gaede, J. Shore, L. Reven, C. R. Bowers, J. Kritzenberger, T. Pietraß, A. Pines, P. Tang, and J. A. Reimer, *J. Am. Chem. Soc.* **115,** 8491 (1993).
9. N. D. Bhaskar, W. Happer, and T. McClelland, *Phys. Rev. Lett.* **49,** 25 (1982).
10. W. Happer, E. Miron, S. Schaefer, D. Schreiber, W. A. van Wijngaarden, and X. Zeng, *Phys. Rev. A* **29,** 3092 (1984).
11. M. S. Albert, G. D. Cates, B. Driehuys, W. Happer, B. Saam, C. S. Springer, Jr., and A. Wishnia, *Nature* **370,** 199 (1994).
12. H. Middleton, R. D. Black, B. Saam, G. D. Cates, G. P. Cofer, B. Guenther, W. Happer, L. W. Hedlund, G. A. Johnson, K. Juvan, and J. Swartz, *Magn. Reson. Med.* **33,** 271 (1995).
13. B. Driehuys, G. D. Cates, W. Happer, H. Mabuchi, B. Saam, M. S. Albert, and A. Wishnia, *Phys. Lett. A* **184,** 88 (1993).
14. D. Raftery, L. Reven, H. Long, A. Pines, P. Tang, and J. Reimer, *J. Phys. Chem.* **97,** 1649 (1993).
15. X. Zeng, E. Miron, W. A. van Wijngaarden, D. Schreiber, and W. Happer, *Phys. Lett. A* **96,** 191 (1983).
16. A. Haase, J. Frahm, D. Matthaei, W. Hanicke, and K. D. Merboldt, *J. Magn. Reson.* **67,** 258 (1986).
17. G. A. Barrall, L. Frydman, and G. C. Chingas, *Science* **255,** 714 (1992).
18. S. S. Kistler, *Nature* **127,** 741 (1931).
19. S. J. Teichner, *in* "Aerogels" (J. Fricke, Ed.), Springer-Verlag, Berlin, 1986.
20. R. W. Pekala and F. M. Kong, *Rev. Phys. Appl.* **24**(Supplement 4), 33 (1989).
21. P. H. Tewari, A. J. Hunt, and K. D. Lofftus, *Mat. Lett.* **3,** 363 (1985).
22. P. Mansfield and I. L. Pykett, *J. Magn. Reson.* **29,** 355 (1978).
23. P. Mansfield, *J. Phys. C.* **10,** L55 (1977).